



Chemistry of bone remodelling preserved in extant and fossil Sirenia

Journal:	<i>Metallomics</i>
Manuscript ID	MT-ART-12-2015-000311.R1
Article Type:	Paper
Date Submitted by the Author:	22-Feb-2016
Complete List of Authors:	Anné, Jennifer; University of Manchester, School of Earth, Atmospheric and Environmental Science Wogelius, Roy; University of Manchester, School of Earth, Atmospheric and Environmental Science Edwards, Nicholas; University of Manchester, School of Earth, Atmospheric and Environmental Science van Veelen, Arjen; University of Manchester, School of Earth, Atmospheric and Environmental Science Ignatyev, Konstantin; Diamond Light Source, Manning, Phillip; University of Manchester, School of Earth, Atmospheric and Environmental Science; College of Charleston, Department of Geology and Environmental Geoscience

1
2
3
4
5
6
7
8
9
10
11
12
13
14
15
16
17
18
19
20
21
22
23
24
25
26
27
28
29
30
31
32
33
34
35
36
37
38
39
40
41
42
43
44
45
46
47
48
49
50
51
52
53
54
55
56
57
58
59
60

1 **Chemistry of bone remodelling preserved in extant and fossil Sirenia**

2

3 Jennifer Anné*^{1,2}, Roy A. Wogelius^{1,2}, Nicholas P. Edwards^{1,2}, Arjen van Veelen¹, Konstantin

4 Ignatyev³, Phillip L. Manning^{2,4}

5

6 ¹University of Manchester, School of Earth, Atmospheric and Environmental Sciences, Williamson

7 Research Centre for Molecular Environmental Science, Manchester M13 9PL, UK

8 ²University of Manchester, Interdisciplinary Centre for Ancient Life, Manchester, M13 9PL, UK

9 ³Diamond Light Source, Didcot, OX11 0DE, UK

10 ⁴Department of Geology and Environmental Geoscience, College of Charleston, 66 George St,

11 Charleston, SC 29424, USA

12

13

14 *jennifer.anne@manchester.ac.uk

15

16 **Abstract**

17 Bone remodelling is a crucial biological process needed to maintain elemental homeostasis. It is
18 important to understand the trace elemental inventories that govern these processes as malfunctions in
19 bone remodelling can have devastating effects on an organism. In this study, we use a combination of
20 X-ray techniques to map, quantify, and characterise the coordination chemistry of trace elements
21 within the highly remodelled bone tissues of extant and extinct Sirenia (manatees and dugongs). The
22 dense bone structure and unique body chemistry of sirenians represent ideal tissues for studying both
23 high remodelling rates as well as unique fossilisation pathways. Here, elemental maps revealed
24 uncorrelated patterning of Ca and Zn within secondary osteons in both extant and fossil sirenians, as
25 well as elevated Sr within the connecting canals of fossil sirenians. Concentrations of these elements
26 are comparable between extant and fossil material indicating geochemical processing of the fossil
27 bone has been minimal. Zn was found to be bound in the same coordination within the apatite
28 structure in both extant and fossil bone. Accurate quantification of trace elements in extant material
29 was only possible when the organic constituents of the bone were included. The comparable
30 distributions, concentrations, and chemical coordination of these physiologically important trace
31 elements indicate the chemistry of bone remodelling has been preserved for 19 million years. This
32 study signifies the powerful potential of merging histological and chemical techniques in the
33 understanding of physiological processes in both extant and extinct vertebrates.

35 **Introduction**

36 The processes that govern bone physiology utilise a suite of trace elements that can be correlated to
37 specific biosynthetic pathways.¹⁻³ By mapping and quantifying these trace elements, we can gain a
38 better understanding of these processes and the variation between different tissue types. In addition,
39 the trace elements inventories associated with bone physiology have been shown to preserve in other
40 fossil bone tissues, suggesting the physiology of bone remodelling can be preserved over millions of
41 years.³ Thus the combination of morphological and chemical preservation allows for a more in depth
42 understanding of the physiology of extinct organisms.

44 ***Bone Remodelling***

45 The dynamic state of bone results in a high turnover of material through remodelling, allowing the
46 body to cope with changing stresses (shape of bone) and to release essential trace elements held
47 within the apatite structure for use in other biological processes (e.g. growth, healing, pregnancy,
48 etc.).⁴⁻⁶ Histologically, remodelled bone can be observed as Haversian systems; a dense network of
49 secondary osteons (a function of the remodelling process) usually observed in older individuals.^{4,6}
50 These systems represent a complicated network of osteons and connecting canals (canals connecting
51 osteons) that are heterogenous in their distribution due to the differential stresses and movement of

1
2
3 52 bone material. Haversian systems are of biological interest as they provide target areas for the study of
4 53 active bone resorption and deposition.⁴⁻⁶ If this deposition/resorption cycle is not heavily regulated, it
5
6 54 can have a devastating impact on an organism. The pathways and signalling that moderate the cycle of
7
8 55 bone deposition and resorption utilise specific trace elements in their regulation including copper,
9 56 zinc, and strontium.¹⁻³ Because the degree and distribution of bone deposition/resorption is so varied
10 57 within the bone tissue, the distributions of these elements can also fluctuate. Thus it is important to
11 58 look at a larger surface area (at the millimetre scale) of both the morphology and chemistry rather than
12 59 focusing on single histological features (micron).
13
14
15
16

17 61 In the Sirenia (dugongs and manatees) the degree of bone deposition and remodelling is taken to the
18 62 extreme in a condition known as pachyosteosclerosis, which results in exceedingly dense ribs used for
19 63 counter buoyancy.⁷⁻⁸ This unique tissue type makes sirenians an ideal group to study the differential
20 64 trace element uptake during remodelling as it represents an extreme example of this physiological
21 65 process. Sirenians also represent a unique aspect of trace element hyperaccumulation as they have
22 66 been shown to have unique chemical inventories within soft tissues due to a low Cu diet.⁹ However, it
23 67 has not been shown how such trace element inventories are accumulated, maintained and recycled in
24 68 sirenian bone tissue.⁹⁻¹⁰
25
26
27
28
29

30 70 *Haversian Systems and Fossilisation*

31
32 71 The extremely dense skeleton of Sirenia also present a unique taphonomic condition as the compact
33 72 bone impedes the diffusion of ground waters compared to the skeleton of other vertebrates. Diffusion
34 73 models have viewed bone as a homogenous medium, with the only pathway by which groundwater
35 74 could interact being through surface interactions.¹¹⁻¹² However, bone tissue is highly variable in both
36 75 porosity, structure and chemistry, with many micro pores and fractures that increase the pathways and
37 76 surface area that interact with ground water. In sirenians, the most likely mode of diagenetic alteration
38 77 is through the complex system of connecting canals within the Haversian system, which offer one of
39 78 the few ways for pore water to penetrate into dense bone through the connecting canals between
40 79 osteons.¹³⁻¹⁴ The complexity of the interconnectivity and distribution of these canals can make it
41 80 difficult to determine the distribution of diagenetic alteration through the use of point analyses.¹¹⁻¹⁵
42 81 Thus the ability to map over larger surface areas allows for the visualisation of such complex
43 82 chemical pathways that would impact fossilisation, including the vast network of micro pores
44 83 associated with osteocyte cell networks and Haversian systems¹⁶ In addition, although there are many
45 84 diagenetic factors that can alter the chemistry of a fossil, it is possible to differentiate between original
46 85 organismal (endogenous) chemistry and environmentally mediated (exogenous) material through
47 86 spectroscopy.
48
49
50
51
52
53
54
55
56
57
58
59
60

1
2
3 88 In this study we look at morphological and chemical characterisations of dense bone in extant
4 89 (*Trichechus manatus*) and extinct (*Metaxytherium sp.*) sirenians to 1) identify the chemical
5 90 inventories in remodelled bone; 2) see if biomarkers for bone turnover can be preserved in the fossil
6 91 record; 3) identify the degree and pathway of diagenetic alteration within extremely dense bone
7 92 tissues.
8
9

10 93 11 12 94 **Methods**

13 95 ***Optical Histology***

14
15 96 Histological sections were used to identify tissue types and to select areas of interest for microfocus
16 97 mapping. A section of rib from the extant (*T. manatus*; West Indian manatee; NMS.Z 2015.9; Figures
17 98 S1) and extinct (*Metaxytherium*; PAS11-04; Late Miocene, USA; Figure S2) sirenian ribs were thin
18 99 sectioned using the petrographic facilities at the School of Earth, Atmospheric and Environmental
19 100 Sciences (University of Manchester). Thin sections were polished to a thickness of ~ 50µm. The thin
20 101 sections were subject to optical histological analysis using a Nikon petrographic microscope with a
21 102 camera attachment and viewed under normal and cross-polarised light at 4, 10 and 20x magnification.
22
23
24
25
26

27 104 ***Synchrotron analysis***

28
29 105 The source billets from the thin sections of extant (*T. manatus*; Figure S1) and fossil
30 106 (*Metaxytherium*; Figure S2) samples were retained and used for analysis by chemical methods. A
31 107 complementary set of analyses were obtained for both the extant and fossil specimens via synchrotron
32 108 X-Ray Fluorescence (XRF) elemental mapping, EDS quantification and Extended X-ray Absorption
33 109 Fine Structure (EXAFS) spectroscopy. No additional sample preparation was performed (embedding,
34 110 polishing, etc.) as such procedures could skew chemical results. Elemental mapping was used to
35 111 visualise elemental distributions over the various types of histological features identified in optical
36 112 thin section. Elemental quantification was performed to test whether trace metal concentrations were
37 113 comparable between the extant and fossil material. EXAFS was used to determine if the local
38 114 chemical bonding environment of Zn in extant bone was preserved within the fossil.
39
40
41
42
43
44

45
46 116 Specimens were mapped at the microfocus beamline I-18 at the Diamond Light Source (DLS,
47 117 Oxfordshire, UK), which allows for high resolution (2-10µm) scans of areas of interest (millimetre
48 118 scale). This beamline can operate at high incident beam energies (>20 keV), which enables efficient
49 119 excitation of Sr ($E_c = 16.1$ keV) and thus allows the mapping and quantification of this critically
50 120 important component of bone. Specimens were mapped at an incident beam energy of 17 keV (flux
51 121 10^{10} - 10^{11} photons s^{-1}) using a beam size of 5.5 µm produced via Kirkpatrick-Baez focusing mirror.
52 122 The sample was mounted on an x-y-z translation stage using an SEM carbon tab and raster scanned at
53 123 a 45° angle to the incident X-ray beam with a four element Si drift Vortex fluorescence detector set at
54
55
56
57
58
59
60

1
2
3 124 90° scattering angle.^{3, 17-18} Mapping, point analyses, and EXAFS at beamline I18 is completed for
4 125 high atomic weight elements (Ca and higher) in air. Maps were processed using the ROI imaging tool
5 126 in PyMCA freeware¹⁹ by defining the X-ray emission energy of an element in the recorded EDS
6 127 spectra.
7
8

9 128
10 129 Quantification was accomplished by taking a full EDS spectrum for 30 seconds at locations of interest
11 130 revealed through XRF mapping. Three measurements are taken for each location to account for
12 131 heterogeneity within the bone tissue. EDS spectra were fit using PyMCA, calibrated using a Durango
13 132 apatite mineral standard, and well-constrained using previous quantification data.^{3, 17-19} Concentrations
14 133 obtained using this method were compared with concentrations obtained from PIXE/RBS analysis.
15
16
17
18

19 134
20 135 Full Zn K-edge EXAFS were collected for both extant and fossil material to $k = 12$. The energy of the
21 136 Zn K-edge was calibrated using a Zn-foil. Background subtraction, data normalization and fitting of
22 137 the EXAFS were performed using (d)Athena and (d)Artemis version 0.9.20.²⁰
23
24

25 138

26 139 ***Particle-Induced X-ray Emission (PIXE)/Rutherford Backscattering Spectroscopy (RBS)***

27 140 Conversion of X-ray yield intensity to concentration is complicated by uncertainties regarding matrix
28 141 composition. Even using the He-purge system, the attenuation of low energy characteristic X-rays
29 142 from the light elements that dominate organic compounds (especially C, N, O) precludes their
30 143 analysis at beamline I18. Therefore in order to improve our knowledge of matrix composition and
31 144 thereby improve the accuracy of our trace element quantification we performed complementary
32 145 particle beam analysis on the extant sample (*T. manatus*). PIXE and RBS analyses were used to
33 146 directly measure and map the light element concentrations so that accurate matrix compositions could
34 147 then be used to refine the XRF results. PIXE/RBS was performed at the Surrey Ion Beam Centre
35 148 (University of Surrey, Guildford, UK). The setup here allows for both PIXE and RBS data to be taken
36 149 simultaneously, yielding a combination of fluorescence spectra for elemental quantification and depth
37 150 profile information which is especially sensitive to proton backscattering from light elements.

38 151 PIXE/RBS thus allows for the quantification of organic content within the bone, which is not possible
39 152 using the synchrotron setup at DLS. Due to the high probability of charge build-up with thick
40 153 sections, thin sections were used instead of the thicker bone billet. The thin section was carbon coated
41 154 (~10 nm), mounted using double-sided carbon tape, and inserted into the vacuum chamber which
42 155 contained both an X-ray and particle detector. Specimens were mapped using a 2.5 MeV proton beam
43 156 (2MV Tandetron accelerator), with a beam size of 6 x 10 μm . Concentrations were calculated using
44 157 the raw X-ray and RBS data using a combination of the OMDAQ2007 and GUPIXWIN programs²¹
45 158 using a Pb glass and Durango apatite standards for calibration of beam parameters. The statistical and
46
47
48
49
50
51
52
53
54
55
56
57
58
59
60

1
2
3 159 fitting error for elemental concentrations was calculated by GUPIXWIN using the peak and
4 160 background counts for each element.
5
6

7 161

8 162 **Results**

9 163 Figure 1 shows the similarities in both histology and trace element distributions between the extant (*T.*
10 164 *manatus*) and fossil (*Metaxytherium*) samples. Optical light histology shows tissue types consisting
11 165 mainly of a dense mixture of primary and secondary osteon (white circle). These features are
12 166 identified by the circular pattern of the lacunae (small space containing an osteocyte), seen in optical
13 167 histology as small, elongated black dots. In the elemental maps of Ca, a bright (relatively higher
14 168 concentration) ‘comet tail-like’ structure extends from the secondary osteon in both specimens
15 169 (highlighted insert), indicating the size and shape of the cutting cone. Elemental maps of Zn show
16 170 elevated concentrations within the infilled bone tissue of the secondary osteons (extant and fossil; red
17 171 circle) and the lining of the connecting canals (extant; red arrow). The only difference in elemental
18 172 distributions between extant and fossil material is seen in Sr, which is concentrated within the
19 173 connecting canals of the fossil (red arrow) and as a wash within extant material.
20
21
22
23
24
25
26

27 174

28 175 For extant material (*T. manatus*), the concentrations obtained through synchrotron analysis are
29 176 consistent with those obtained by PIXE/RBS. The collagen-apatite ratio was calculated at 1:3 (~33%
30 177 collagen) based on RBS profiles (Figure S3). Dismissing the effect of collagen on trace element
31 178 calculation resulted in large quantification errors, resulting in improbable (potentially toxic)
32 179 concentrations (Table S1). Elemental concentrations were comparable between extant and extinct
33 180 specimens when collagen was included in the stoichiometry with the exception of highly elevated Mn
34 181 and Fe in the fossil (Table 1).
35
36
37

38 182

39 183 EXAFS revealed Zn to be in tetrahedral coordination with four oxygens at 1.95 Å in both extant and
40 184 fossil samples (Figure 2; Table 2). This is consistent with Zn substituting into the Ca² site, similar to
41 185 the Zn coordination found in both bio and non-bio Zn-HAP.²²⁻²³ The k-space data for each are similar
42 186 with peaks aligned at 2, 4, 6, 8, and 10 Å⁻¹. After Fourier-Transforming the data, Figure 2B shows how
43 187 the first shell arrangements of atoms around the central Zn absorber is virtually the same in both
44 188 specimens.
45
46
47

48 189

49 190 **Discussion**

50 191 Elemental mapping revealed trace elements associated with bone remodelling (Ca and Zn) to be
51 192 concentrated within discrete histological features of dense Haversian bone in the Sirenians, *T.*
52 193 *manatus* (NMS.Z 2015.9) and *Metaxytherium* (PAS11-04). Such imaging could only be resolved
53 194 using the combined sensitivity and resolution of synchrotron-based mapping. Ca distributions are seen
54
55
56
57
58
59
60

1
2
3 195 as comet tail-like structures interpreted here as the three-dimensional structure of the cutting cone in
4 196 both extant and fossil samples. An alternative interpretation of these features is a shadow effects
5
6 197 caused by beam geometry. However, as these features are only present in certain elements and not all,
7
8 198 the more likely cause is enrichment by biological processes. Pooling of Ca within the cutting cone can
9
10 199 be attributed to osteoblastic regulation of mineralisation during deposition, where osteoblasts
11
12 200 membrane-bound matrix vesicles concentrate Ca and P.²⁴ Elevated Ca could also be caused by an
13
14 201 increase of free Ca released from the bone during the resorption stage of remodelling.^{4,6}
15
16 202

17
18 203 Elemental maps of Zn revealed higher concentrations within the lining of the connecting canals
19
20 204 between osteons (NMS.Z 2015.9) and around secondary osteons within the Haversian system (both).
21
22 205 This is similar to findings in previous studies on human osteons as Zn is known to pool in forming
23
24 206 osteons, especially within the area of osteoid at the mineralisation front.^{1-2,25} The overall elevated
25
26 207 concentrations of Zn alludes to the heavy demand for bone-regulating trace elements within
27
28 208 remodelled bone, with Zn playing a crucial role in healthy bone development.²⁶ Elevated levels of Zn
29
30 209 also fits with the findings of high Zn in the liver of extant *Dugong dugon*, where Zn was found in
31
32 210 concentrations of up to 4 wt%.⁹ Concentrations of Zn are comparable between extant and fossil bone,
33
34 211 indicating Zn has not been significantly added or lost during fossilisation. Zn EXAFS of the fossil
35
36 212 bone is comparable to the coordination seen in the extant manatee (Figure 2), strongly supporting the
37
38 213 conclusion that the Zn in the fossil bone is endogenous and the observed distribution of Zn has been
39
40 214 preserved through deep time.
41
42 215

43
44 216 Sr is elevated in both extant and fossil manatee bone samples compared to normal bone
45
46 217 concentrations previously determined in the bones of other marine mammals, however the levels
47
48 218 found here are within the concentration range measured in extant dugong tusks (1709-2155 ppm).^{10,26-}
49
50 219 ²⁸ Elevated levels of Sr in manatee bone may be attributed to two factors. Firstly, Sr concentrations
51
52 220 tend to be high for bone grown within from marine environments. Secondly, Sr concentrations tend to
53
54 221 be higher in herbivores versus carnivores²⁶ for species from the same environment. Therefore
55
56 222 manatees, as marine herbivores, would be expected to have relatively high Sr contents in their bones.
57
58 223 Furthermore, high Sr is expected in bone versus soft tissue as the biological deposition of Sr is almost
59
60 224 exclusively within bone, where it substitutes for Ca in mineralized tissue.²⁸⁻²⁹ Sr is also known to
225 concentrate in areas of high rates of remodelling and repair as it is an important element in the
226 regulation of osteoclasts.^{25,29} We also note that the connecting canals of PAS11-04 are preferentially
227 enriched in Sr, highlighting the detailed connectivity of the complex Haversian system (Figure 1). The
228 Sr enrichment at the surfaces of the connecting canals may be due to biological substitutions as
229 discussed above, or it may also reflect post-mortem mass transfer of Sr into the exposed internal canal

1
2
3 230 surfaces from geochemical fluids, because Haverisan systems may provide ground water infiltration
4 231 pathways during diagenesis.¹¹
5
6

7 232
8 233 Elemental concentrations calculated for NMS.Z 2015.9 are within the expected range for marine
9 234 vertebrates.^{8-9, 25,27} Most importantly, it was found that the inclusion of organic components within the
10 235 matrix stoichiometry in the fit calculations greatly affected and improved trace element quantification
11 236 (Figure S3). This was most noticeable in Zn, which was initially highly elevated compared to known
12 237 biological concentrations from both PIXE and synchrotron analysis when collagen was not included
13 238 in the experimental parameters (sample matrix stoichiometry; Table S1). This affect was not seen in
14 239 previous analyses of extant material,³ however, all previous studies have been conducted mainly on
15 240 avian material, which in museum collections can dry quickly due to the thinness of the bone and low
16 241 concentrations of marrow. We suggests then that the thickness and density of the sirenean bone may
17 242 have allowed it to retain more of its organic constituents and we caution future studies that apply
18 243 chemical techniques to bone that remove or do not take into account organics for matrix
19 244 stoichiometry.
20
21
22
23
24
25
26

27 246 **Conclusion**

28 247 The combination of detailed morphological and chemical analyses resulted in the imaging of bone
29 248 remodelling pathways in both extinct and extant Sirenia. Elemental mapping of remodelled bone in *T.*
30 249 *manatus* revealed strong correlations between histological features and the elements Ca and Zn. These
31 250 distributions highlight morphological features and provide evidence for active physiological processes
32 251 occurring up to the time of death. In particular Zn is found around areas of active ossification. The
33 252 same trace element distributions are seen in a fossil Sirenian, *Metaxytherium*, indicating that original
34 253 biochemistry has been preserved for ~19 million years. Elemental mapping also reveals complex
35 254 histological structures such as connecting canals; features that cannot be seen in optical microscopy.
36 255 Thus the application of synchrotron-based elemental imaging and spectroscopy combined with optical
37 256 histological analyses can be used to not only strengthen the correlation between morphology and
38 257 physiological processes, but also help visualise and provide a better understanding of how bone tissue
39 258 morphology and chemistry can affect fossilisation pathways.
40
41
42
43
44
45
46
47

48 259 49 260 **ACKNOWLEDGEMENTS**

50 261 We thank Dr. Peter Dodson of the University of Pennsylvania, the Surrey Ion Beam Centre and Dr. G.
51 262 Grime (University of Surrey), NERC (NE/J023426/1), STFC, the Jurassic Foundation (awarded J.A.)
52 263 the University of Manchester Dean's Fund (awarded J.A.), the Diamond Light Source for access to
53 264 beamline I18 (SP8597, SP9488-1), and the reviewers for their insightful comments. Prof. Manning
54 265 thanks STFC for their continued support at both the Diamond Lightsource and the STFC PE Fellows.
55
56
57
58
59
60

267 REFERENCES

- 268 1. S. Gomez, R. Rizzo, M. Pozzi-Mucelli, E. Bonucci and F. Vittur, *Bone*, 1999, 25(1), 33-38.
- 269 2. S. Haumont, *J. Histochem. Cytochem.*, 1960, 9, 141-145.
- 270 3. J. Anné, N.P. Edwards, R.A. Wogelius, A.R. Tumarkin-Deratzian, W.I. Sellers, A. van
- 271 Veelen, U. Bergmann, D. Sokaras, R. Alonso-Mori, K. Ignatyev, V.M Egerton and P.L.
- 272 Manning, *J. R. Soc. Interface*, 2014, 11(96), 20140277–20140277.
- 273 4. L.G. Raisz, *Clin. Chem.*, 1999, 45(8B), 1353-1358.
- 274 5. R.F.M. van Oers, R. Ruimerman, E. Tanck, P.A.J. Hilbers and R. Huiskes, *Bone*, 2008, 42,
- 275 250-259.
- 276 6. N.B. Watts, *Clin. Chem.*, 1999, 45(8B), 1359-1368.
- 277 7. V. Buffrénil, A. Canoville, R. D’Anastasio and D.P. Domning, D.P., *J. Mamm. Evol.*, 2010,
- 278 17(2), 101–120.
- 279 8. D.P. Domning and V. Buffrénil, *Mar. Mammal Sci.*, 1991, 7(4), 331–368.
- 280 9. G.R.W. Denton, H. Marsh, G.E. Heinsohn and C. Burdon-Jones, *Mar. Bio.*, 1980, 57(3), 201–
- 281 219.
- 282 10. J.S. Edmonds, Y. Shibata, R.I.T. Prince, A.R. Preen and M. Morita, *Mar. Bio.*, 1997,
- 283 129(2), 203–214.
- 284 11. M.J. Kohn, *Geochim. Cosmochim. Ac.*, 2008, 72 (15), 3758–70,
- 285 doi:10.1016/j.gca.2008.05.045
- 286 12. M.J. Schoeninger, K.M. Moore, M.L. Murray and J.D. Kingston, *Appl. Geochem.*, 1989, 4,
- 287 281-292.
- 288 13. M.J. Kohn and R.J. Moses, *Proc. Nat. Acad. Sci USA*, 2013, 110 (2), 419–24,
- 289 doi:10.1073/pnas.1209513110.
- 290 14. M.B. Goodwin, P.G. Grant, G. Bench. and P.A. Holroyd, *Palaeogeograph. Palaeoclimat.*
- 291 *Palaeoecol.*, 2007, 253 (3-4), 458–76, doi:10.1016/j.palaeo.2007.06.017.
- 292 15. D. Herwartz, T. Tütken, K.P. Jochum and P.M. Sander, *Geochim. Cosmochim. Act.*, 2013,
- 293 103, 161–83, doi:10.1016/j.gca.2012.10.038.
- 294 16. B. Hesse, P. Varga, M. Langer, A. Pacureanu, S. Schrof, N., Männicke, H. Suhonen, P.
- 295 Maurer, O. Cloetens, F. Peyrin and K. Raum. *J Bone Miner Res.*, 2015, 30(2), 346-56, doi:
- 296 10.1002/jbmr.2324.
- 297 17. V.M. Egerton, R.A. Wogelius, M.A. Norell, N.P. Edwards, W.I. Sellers, U. Bergman, D.
- 298 Sokras, R. Alonso-Mori, K. Ignatyev, A. van Veelen, J. Anné, B. van Dongen, F. Knoll and
- 299 P.L. Manning, *J. Anal. At. Spectrom.*, 2015, 30, 627-34.
- 300 18. N.P. Edwards, P.L. Manning, U. Bergmann, P.L. Larson, B.E. van Dongen, W.I. Sellers, S.M.
- 301 Webb, D. Sokaras, R. Alonso-Mori, K. Ignatyev, H.E. Barden, A. van Veelen, J. Anné, V.M.
- 302 Egerton and R.A. Wogelius, *Metallics*, 2014, 6(4), 774.

- 1
2
3 303 19. V.A. Solé, E. Papillon, M. Cotte, P.H. Walter, and J. Susini, *Spectrochim. Acta B*, 2007, 62,
4 304 63-68.
5
6 305 20. B. Ravel and M. Newville, *J. Synchrotron Rad.*, 2005, 12, 537-541.
7
8 306 21. J.A. Maxwell, W.J. Teesdale and J.L. Campbell, *Nucl. Instrum. Methods Phys. Res., Sect. B.*,
9 307 1995, 95(3), 407-421.
10
11 308 22. D. Bazin, X. Carpentier, I. Brocheriou, P. Drofmmuller, S. Aubert, C. Chappard, D. Thiaudière,
12 309 S. Reguer, G. Waychunas, P. Jungers and M. Daudon, *Biochimie*, 2009, 91, 1294-1300.
13
14 310 23. Y. Tang, H.F. Chappell, M.T. Dove, R.J. Reeder and Y.J. Lee, *Biomaterials*, 2009, 30(15),
15 311 2864–2872.
16
17 312 24. B. Clarke, *Clin. J. Am. Soc. Nephrol.*, 2008, 3(Suppl. 3), S131-S139
18
19 313 25. B. Pemmer, A. Roschger, A. Wastl, J.G. Hofstaetter, P. Wobrauschek, R. Simon, H.W.
20 314 Thaler, P. Roschger, K. Klaushofer and C. Strelly, *Bone*, 2013, 57, 184-193.
21
22 315 26. R. Eisler, *Compendium of Trace Metals and Marine Biota*, Elsevier Science, Oxford UK.,
23 316 2009.
24
25 317 27. J.C. Sealy and A. Sillen, *J. Archaeol. Sci.*, 1988, 15, 425-438
26
27 318 28. Y. Fujise, K. Honda, R. Tatsukawa and S. Mishima, *Mar. Pollut. Bull.*, 1988, 19(5), 226–230.
28
29 319 29. T. Swanston, T. Varney, I. Coulthard, R. Feng, B. Brewer, R. Murphy, C. Hennig and D.
30 320 Cooper, *J. Archaeol. Sci.*, 2012, 39(7), 2409–13, doi:10.1016/j.jas.2012.01.041.
31 321

322 TABLES AND TABLE CAPTIONS

Element	Synchrotron				PIXE		
	Durango Standard	<i>T. manatus</i>		<i>Metaxytherium</i>		Durango Standard	<i>T. manatus</i> Bulk
Ca	38.19%	40.34%	39.86%	31.32%	32.31%	46.01%	42.26%
Mn	-	11	18	175	190	-	-
Fe	397	72	117	6317	7217	333 (7.7)	94 (2.9)
Ni	-	8	9	21	27	-	100 (12.2)
Cu	-	11	18	36	44	-	26 (10.4)
Zn	27	244	477	161	234	35 (35.3)	340 (1.7)
As	797	3	3	9	15	839 (5.3)	-
Sr	669	1326	1444	3105	3204	982 (9.9)	1338 (2.2)

323 Table 1: Quantification of trace elements in *T. manatus* using synchrotron and PIXE analyses and
 324 *Metataxytherium* using synchrotron analyses. “Osteon” refers to the cylindrical compact bone tissue
 325 around the Haversian canal openings. “Bone” refers to all other bone tissues. Concentrations are given
 326 in ppm or weight percent (wt%). Conservative 2σ error for all DLS data as well as Ca via PIXE are
 327 $\sim 10\%$ of the absolute value. Error estimates for PIXE trace metals are given as percent error (%).

328

Specimen	Path	CN	R(\AA)	$\sigma^2(\text{\AA}^2)$	$\Delta E_0(\text{eV})$	S^2	χ^2	R
<i>T. manatus</i>	Zn-O	4.4	1.95(07)	0.007(1)	1.95 ± 0.77	0.99(3)	92	0.01
<i>Metataxytherium</i>	Zn-O	4.4	1.97(04)	0.009(08)	2.32 ± 0.39	1.00(4)	17.82	0.019

329 Table 2: Fit statistics for Zn EXAFS in *T. manatus* and *Metataxytherium* using (d)Artemis. Errors are
 330 given as (\pm) the last significant figure unless specified. Error for CN is 25%.

331

332 FIGURE CAPTIONS

333

334 Figure 1: Optical thin sections of *T. manatus* (NMS.Z 2015.9) and *Metaxytherium* (PAS11-04)
335 compared to microfocus (DLS) elemental maps of Ca, Zn and Sr. Histological views are represented
336 in cross-polarized light (*Metaxytherium*) with a lambda filter (*T. manatus*). Extant and fossil material
337 is comparable in both optical histology and elemental distributions with the exception of Sr. Optical
338 histology shows primary and secondary osteons (examples highlighted in white inserts). The extent of
339 the cutting cones can be observed in Ca as ‘comet tails’ coming off the opening of the secondary
340 osteon (examples highlighted in white inserts). Zn is concentrated within bone deposited within the
341 secondary osteons (examples circled in red), and along the lining of connecting canals between
342 osteons (red arrow). Sr is relatively evenly distributed throughout the bone tissue in the extant *T.*
343 *manatus* specimen, but is concentrated within the connecting canals of the fossil specimen (example
344 highlighted with red arrow). Scale is 1 mm.

345

346 Figure 2: Zn EXAFS for *Metaxytherium sp.* and *T. manatus* showing EXFAS k-space data (black
347 curve) with fit (red curve) along with the (b) Fourier transformed R-space results (data = black curve;
348 fit = red curve). The coordination chemistry of Zn in this fossil and in the extant bone is the same.

1
2
3
4
5
6
7
8
9
10
11
12
13
14
15
16
17
18
19
20
21
22
23
24
25
26
27
28
29
30
31
32
33
34
35
36
37
38
39
40
41
42
43
44
45
46
47
48
49
50
51
52
53
54
55
56
57
58
59
60

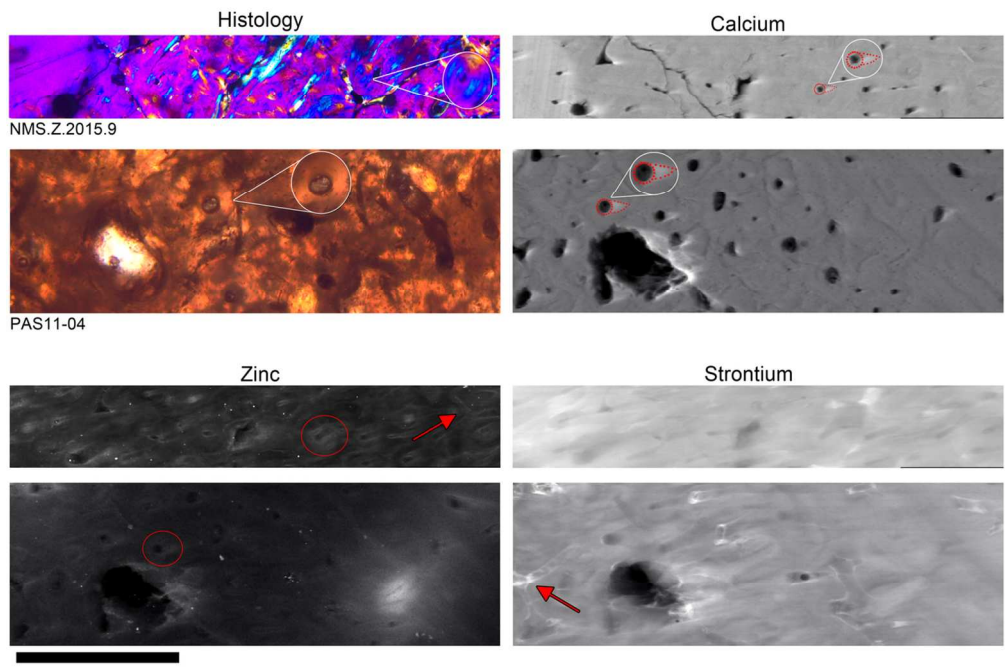


Figure 1: Optical thin sections of *T. manatus* (NMS.Z 2015.9) and *Metaxytherium* (PAS11-04) compared to microfocus (DLS) elemental maps of Ca, Zn and Sr.
118x80mm (300 x 300 DPI)

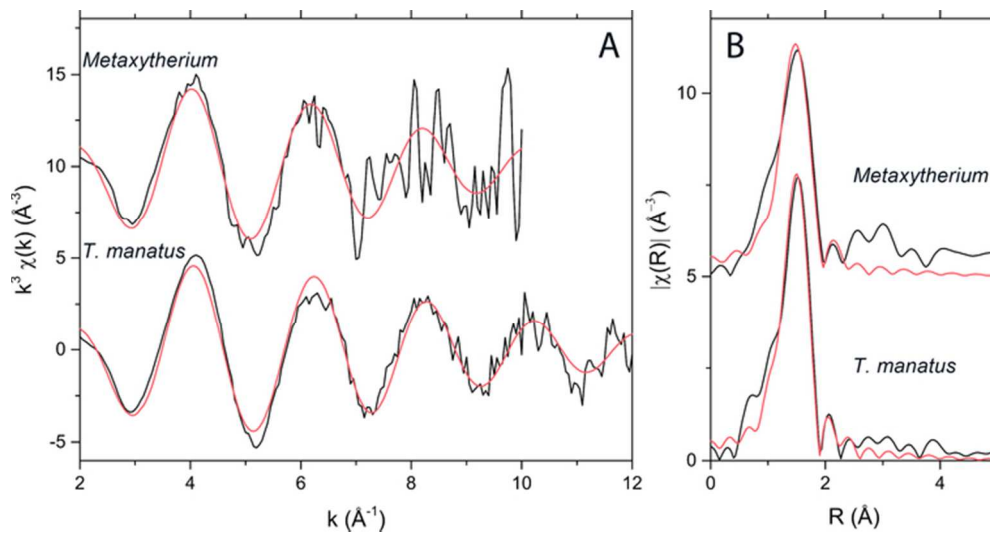


Figure 2: Zn EXAFS for *Metaxytherium* sp. and *T. manatus* showing EXFAS k-space data (black curve) with fit (red curve) along with the (b) Fourier transformed R-space results (data = black curve; fit = red curve).
 65x33mm (300 x 300 DPI)

1
2
3
4
5
6
7
8
9
10
11
12
13
14
15
16
17
18
19
20
21
22
23
24
25
26
27
28
29
30
31
32
33
34
35
36
37
38
39
40
41
42
43
44
45
46
47
48
49
50
51
52
53
54
55
56
57
58
59
60